

Generalized analytic signals in image processing: Comparison, theory and their applications

Swanhild Bernstein, Jean-Luc Bouchot, Martin Reinhardt and Bettina Heise

Abstract. This article is intended as both a mathematical overview of the generalizations of analytic signals to higher dimensional problems as well as their applications and comparisons on artificial and real-world image samples.

We first start by reviewing the basic concepts behind analytic signal theory and derive its mathematical background based on boundary value problems of one dimensional analytic functions. Based on that, two generalizations are motivated by means of higher dimensional complex analysis or Clifford analysis. Both approaches are proven to be valid generalizations of the known analytic signal concept.

In a last part we experimentally motivate the choice of such higher dimensional analytic or monogenic signal representations in the context of image analysis. We see how one can take advantage of one or another representation depending on the application.

Mathematics Subject Classification (2010). Primary 94A12; Secondary 44A12, 30G35.

Keywords. Monogenic signal, monogenic functional theory, image processing, texture, Riesz transform.

1. Introduction

In the past years and since the pioneer work of Gabor [10], the analytic signal has attracted manifold interests in signal processing and information theory. Due to an orthogonal decomposition of oscillating signals into envelope and instantaneous phase or respectively into energetic and structural components, this concept has become very suitable for analyzing signals. In this context such a property is called a split of identity and allows to separate the different characteristics of a signal into useful components.

While this approach has given rise to many one dimensional signal processing methods, other developments have been directed towards higher dimensional generalizations. Of particular interest is the two dimensional case, *i.e.* how to deal with images in an analytic way. As it will be demonstrated in our paper, two main directions have been taken, one based on multidimensional complex analysis and another one based on Clifford analysis.

This article is intended as an overview of the mathematical concepts behind analytic signals based on the Hilbert transform (Sec. 2). Then, the mathematical generalizations are detailed in Sec. 3. The end of that section is dedicated to illustrative examples of the differences between the two generalizations detailed. Sec. 4 describes the use of spinors for image analysis tasks. The last section of this article (Sec. 5) illustrates their applications like demodulation of two dimensional AM-FM signals as provided e.g. in interferometry and some applications in natural images processing.

2. Analytic signal theory and signal decomposition

Analytic signals have been introduced for signal processing in the context of communication theory in the late 40s [10]. Since then, it has shown growing interest as a useful tool for representing real valued signals [23]. We start here by first reviewing the basics about analytic signal theory and Hilbert transform and see how the so-called *split of identity* is an interesting property. In the last part we review the mathematical basics and see how we can derive the analytic signal from a boundary value problem in complex analysis.

2.1. Basic analytic signal theory and the Hilbert transform

Definition 2.1 (1 Dimensional Fourier Transform). In the following, we use as Fourier transform \mathcal{F} :

$$\mathcal{F}(f)(u) = \widehat{f}(u) = \frac{1}{\sqrt{2\pi}} \int_{\mathbb{R}} f(t) e^{-itu} dt \quad (2.1)$$

for $t \in \mathbb{R}, u \in \mathbb{R}$ and $f \in L^2(\mathbb{R})$

Definition 2.2 (Hilbert Transform). The Hilbert transform of a signal $f \in L^2(\mathbb{R})$ (or more generally $f \in L^p(\mathbb{R}), 1 < p < \infty$) is defined either in the spatial domain as a convolution with the Hilbert kernel 2.2 or as a Fourier multiplier 2.3:

$$\mathcal{H}f = h * f \quad (2.2)$$

$$\mathcal{F}(\mathcal{H}f)(u) = -i \operatorname{sign}(u) \mathcal{F}(f)(u) \quad (2.3)$$

where we have made use of two functions:

- The Hilbert kernel $h(t) = \frac{1}{\pi t}$
- The operator $\operatorname{sign}(u) = \begin{cases} 1 & u > 0 \\ 0 & u = 0 \\ -1 & u < 0 \end{cases}$

Following its definition, we notice that the Hilbert transform acts as an asymmetric phase shifting: if we write $\pm i = e^{\pm i\pi/2}$, the phase of the Fourier spectrum of the Hilbert is obtained by a rotation of $\pm 90^\circ$.

Proposition 2.3 (Properties of the Hilbert Transform). *Given a signal f the followings hold true:*

- $\forall u \neq 0, |\mathcal{H}f(u)| = |\mathcal{F}(f)(u)|$
- $\mathcal{H}\mathcal{H}f = -f \Rightarrow \mathcal{H}^{-1} = -\mathcal{H}$

Note that a constant function being not in L^2 can not be reconstructed that way.

The analytic signal is computed as a complex combination of both original signal and its Hilbert transform:

Definition 2.4 (Analytic Signal).

$$f_A = f + i\mathcal{H}f \quad (2.4)$$

Due to its definition, an analytic signal has a one sided Fourier spectrum. And moreover, we have that its values are doubled on the positive side. We can also remark that it is possible to recover the original signal based on its analytic description by taking the real part.

It holds:

Proposition 2.5.

$$\langle f, \mathcal{H}f \rangle_{L_2} = 0 \text{ Orthogonality} \quad (2.5)$$

$$\|f\|_2^2 = \|\mathcal{H}f\|_2^2 \text{ Energy} \quad (2.6)$$

The energy equality is valid only if the DC component of the signal is neglected [9].

Note that it is possible to write the complex analytic signal in polar coordinate. In this case we have: $\forall t \in \mathbb{R}, f_A(t) = A(t)e^{i\phi(t)}$ A is called the local amplitude and ϕ is called the local phase. These local features are defined as follows [10]:

Definition 2.6 (Local features).

$$A(t) = \sqrt{f(t)^2 + \mathcal{H}f(t)^2} \quad (2.7)$$

$$\phi(t) = \arctan \left(\frac{\mathcal{H}f(t)}{f(t)} \right) = \arctan \left(\frac{\Im(f_A(t))}{\Re(f_A(t))} \right) \quad (2.8)$$

Proposition 2.7 (Invariance - equivariance, Split of identity [9]). *The local phase together with the local amplitude fulfill the property of invariance-equivariance:*

- *The local phase depends only on the local structure*
- *The local amplitude depends only on the local energy*

If moreover these features are a complete description of the signal, they are said to perform a split of identity.

However as stated in [9], the split of identity is strictly valid only for band-limited signals with local zero mean property.

If these conditions are fulfilled the analytic signal representation relies on an orthogonal decomposition of the *structural information* (the local phase), and the *energetic information* (the local amplitude).

This split of identity is illustrated on Fig. 1. The first plot represents three signals. They are sine waves generated from a mother sine wave (the red one). The blue curve corresponds to a modification in terms of amplitude of the red one, while the green curve has half the frequency of the red one. Figs. 1(b) and 1(c) are respectively the local amplitudes and phases of these three signals. Note that a small phase shift has been added to the blue curve for better readability. We can clearly see that due to the split of identity, modifying one local characteristic of the signal does not affect the second one and vice versa.

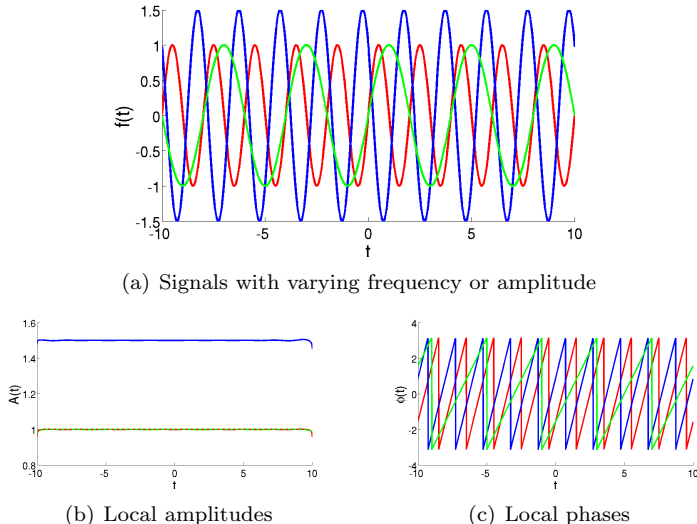


FIGURE 1. Illustration of the split of identity.

2.2. From analytic function to analytic signal

While the analytic signal is a very common concept in the field of signal theory, its basic mathematics can be derived from the theory of analytic functions. The close connection can be understood when considering the following Riemann-Hilbert problem with respect to the complex parameter $z = x + iy$:

$$\frac{\partial F}{\partial z} = 0 \quad z \in \mathbb{C}, y \geq 0, \quad (2.9)$$

$$\Re(F(x)) = f(x) \quad x \in \mathbb{R}. \quad (2.10)$$

One solution of this problem is given by the Cauchy integral

$$F(z) = F_\Gamma f(z) := \frac{1}{2\pi i} \int_{\mathbb{R}} \frac{1}{\tau - z} f(\tau) d\tau. \quad (2.11)$$

Of course this solution is unique only up to a constant. Normally, this constant will be fixed by the condition $\Im(F(z_0)) = c$, i.e. the imaginary part of F given in an interior point.

When we now consider the trace of F_Γ , i.e. the boundary value, we arrive at the so-called Plemelj-Sokhotzki formula:

$$\text{tr } F_\Gamma f = \frac{1}{2}(I + i\mathcal{H})f = \frac{1}{2}f + \frac{1}{2}i\mathcal{H}f =: P_\Gamma f. \quad (2.12)$$

Up to the factor 1/2 this corresponds to our above definition of an analytic signal.

In this way an analytic signal represents the boundary values of an analytic function in the upper half plane (or for periodic functions in the unit disc). Starting from this concept we are going now to take a look at higher dimensional generalizations.

3. Higher dimensional generalizations

Different approaches have been studied in the past years to extend the definition of an analytic signal to higher dimensional spaces. Two of them have gained the greatest interest based respectively on multidimensional complex analysis and Clifford analysis.

3.1. Using multiple complex variables

3.1.1. Mathematics. In 1998 Bülow proposed a definition of a hypercomplex signal based on the so-called partial and total Hilbert transform [5]. To look from our point of view that analytic signals are functions in a Hardy space we consider the following Riemann-Hilbert problem in \mathbb{C}^2 :

$$\frac{\partial F}{\partial \bar{z}_1} = 0 \quad (z_1, z_2) \in \mathbb{C}^2, y_1, y_2 \geq 0, \quad (3.1)$$

$$\frac{\partial F}{\partial \bar{z}_2} = 0 \quad (z_1, z_2) \in \mathbb{C}^2, y_1, y_2 \geq 0, \quad (3.2)$$

$$\Re(F(x_1, x_2)) = f(x_1, x_2) \quad x_1, x_2 \in \mathbb{R}^2. \quad (3.3)$$

For the solution, (see e.g. [7] or [20]), we just want to point out that the domain is a poly-domain in the sense of \mathbb{C}^n , so that we can give it in form of the Cauchy integral:

$$F(z_1, z_2) = \frac{1}{4\pi^2} \int_{\mathbb{R}^2} \frac{1}{(\xi_1 - z_1)(\xi_2 - z_2)} f(\xi_1, \xi_2) d\xi_1 d\xi_2. \quad (3.4)$$

Now again looking at the corresponding Plemelj-Sokhotzki formula we get

$$\begin{aligned} \text{tr } F(x_1, x_2) = & \frac{1}{4} f(x_1, x_2) - \frac{1}{4} \int_{\mathbb{R}^2} \frac{1}{(\xi_1 - x_1)(\xi_2 - x_2)} f(\xi_1, \xi_2) d\xi_1 d\xi_2 \\ & + i \frac{1}{4} \left(\int_{\mathbb{R}} \frac{1}{\xi_1 - x_1} f(\xi_1, x_2) d\xi_1 + \int_{\mathbb{R}} \frac{1}{\xi_2 - x_2} f(x_1, \xi_2) d\xi_2 \right) \end{aligned} \quad (3.5)$$

which up to the factor 1/4 corresponds to the definition of an analytic signal by Hahn [12]. Here

$$\mathcal{H}_i f = \int_{\mathbb{R}} \frac{1}{\xi_i - x_i} f(\xi_i, \cdot) d\xi_1 \quad (3.6)$$

is called the partial Hilbert transform and

$$\mathcal{H}_T f = \frac{1}{4} \int_{\mathbb{R}^2} \frac{1}{(\xi_1 - x_1)(\xi_2 - x_2)} f(\xi_1, \xi_2) d\xi_1 d\xi_2 \quad (3.7)$$

the total Hilbert transform. On the level of Fourier symbols we get

$$\mathcal{F}(\text{tr}F)(u_1, u_2) = (1 + \text{sign}u_1)(1 + \text{sign}u_2)\mathcal{F}f(u_1, u_2). \quad (3.8)$$

Let us now take a look at the definition of Bülow. To this end we consider F to be a function of two variables z_1 and \mathfrak{z}_2 with two different imaginary units \mathbf{i} and \mathbf{j} (with $\mathbf{i}^2 = \mathbf{j}^2 = -1$), i.e. $z_1 = x_1 + iy_1$ and $\mathfrak{z}_2 = x_2 + jy_2$. We remark that both imaginary units can be understood as elements of the quaternionic basis with multiplication rules $\mathbf{i}\mathbf{j} = -\mathbf{j}\mathbf{i} = \mathbf{k}$. In this way the above Riemann-Hilbert problem can be rewritten as

$$\frac{\partial}{\partial \bar{z}_1} F = 0 \quad (z_1, \mathfrak{z}_2) \in \mathbb{C}^2, y_1, y_2 \geq 0, \quad (3.9)$$

$$F \frac{\partial}{\partial \bar{\mathfrak{z}}_2} = 0 \quad (z_1, \mathfrak{z}_2) \in \mathbb{C}^2, y_1, y_2 \geq 0, \quad (3.10)$$

$$\Re(F(x_1, x_2)) = f(x_1, x_2) \quad x_1, x_2 \in \mathbb{R}^2, \quad (3.11)$$

where the second equation should be understood as $\partial_{\bar{\mathfrak{z}}_2}$ being applied from the right due to the non-commutativity of the complex units \mathbf{i} and \mathbf{j} .

The solutions is given by

$$F(z_1, \mathfrak{z}_2) = \frac{1}{4\pi^2} \int_{\mathbb{R}^2} \frac{1}{(\xi_1 - z_1)(\xi_2 - \mathfrak{z}_2)} f(\xi_1, \xi_2) d\xi_1 d\xi_2 \quad (3.12)$$

so that we get from the Plemelj-Sokhotzki formulae

$$\text{tr}F(x_1, x_2) = \frac{1}{4}(I + \mathbf{i}H_1)(I + \mathbf{j}H_2)f(x_1, x_2) \quad (3.13)$$

$$= \frac{1}{4}(f + \mathbf{i}\mathcal{H}_1 f + \mathbf{j}\mathcal{H}_2 f + \mathbf{k}\mathcal{H}_T f)(x_1, x_2). \quad (3.14)$$

While this is now a quaternionic-valued function, it still corresponds to a boundary value of a function holomorphic in two variables. For the representation in Fourier domain one has to keep in mind that now one has to apply one Fourier transform with respect to the complex plane in \mathbf{i} and one Fourier transform with respect to the complex plane generated by \mathbf{j} . Taking into account that $\mathbf{i}\mathbf{j} = -\mathbf{j}\mathbf{i} = \mathbf{k}$ one arrives at the so-called quaternionic Fourier transform [15, 5]:

$$\mathcal{Q}\mathcal{F}f = \int_{\mathbb{R}^2} e^{ix_1\xi_1} f(x_1, x_2) e^{jx_2\xi_2} dx_1 dx_2 \quad (3.15)$$

and the following representation in Fourier symbols

$$\mathcal{Q}\mathcal{F}(\text{tr}F)(u_1, u_2) = (1 + \text{sign}u_1)(1 + \text{sign}u_2)\mathcal{Q}\mathcal{F}f(u_1, u_2) \quad (3.16)$$

3.1.2. Image analysis. In image analysis problems, according to [12] we can introduce the following features

Amplitude. The local amplitude of a multidimensional analytic signal is defined in a similar way as for the one-dimensional case:

$$A_A(x, y) = \sqrt{|f(x, y)|^2 + |\mathcal{H}_1 f(x, y)|^2 + |\mathcal{H}_2 f(x, y)|^2 + |\mathcal{H}_T f(x, y)|^2} \quad (3.17)$$

This is also denoted as *energetic information*

Phase. The phase is a feature describing how much a vector or quaternion number diverge from the real axis. It is defined in a similar manner as for the classical complex plane.

$$\phi_A = \arctan\left(\frac{\sqrt{\mathcal{H}_1 f^2 + \mathcal{H}_2 f^2 + \mathcal{H}_T f^2}}{f}\right) \quad (3.18)$$

This angle ϕ_A is what is denoted as phase or *structural information*.

Orientation. As we are at the moment interested in 2D signals (=images), we can also describe an orientation information, as the principal direction carrying the phase information. The imaginary plane, spanned by $\{i, j\}$, is two-dimensional and therefore we can also define an angle θ_A in this plane:

$$\theta_A = \arctan\left(\frac{\mathcal{H}_2 f}{\mathcal{H}_1 f}\right) \quad (3.19)$$

This new angle is called the orientation of the signal or *geometric information*.

3.2. Using Clifford analysis

Another approach to higher dimensions is the so-called Clifford analysis.

3.2.1. Mathematics. Here we use a so-called Clifford algebra $\mathcal{C}\ell_{0,n}$ [3]. This is the free algebra constructed over \mathbb{R}^n generated modulo the relation

$$x^2 = -|x|^2 \mathbf{e}_0 \quad x \in \mathbb{R}^n \quad (3.20)$$

where \mathbf{e}_0 is the identity of $\mathcal{C}\ell_{0,n}$. For the algebra $\mathcal{C}\ell_{0,n}$ we have the anti-commutation relationship

$$\mathbf{e}_i \mathbf{e}_j + \mathbf{e}_j \mathbf{e}_i = -2\delta_{ij} \mathbf{e}_0, \quad (3.21)$$

where δ_{ij} is the Kronecker symbol. Each element x of \mathbb{R}^n may be represented by

$$x = \sum_{i=1}^n x_i \mathbf{e}_i. \quad (3.22)$$

A first-order differential operator which factorizes the Laplacian is given as the so-called Dirac operator

$$Df(x) = \sum_{j=1}^n \frac{\partial f}{\partial x_j}. \quad (3.23)$$

The Riemann-Hilbert problem for the Dirac operator can be stated in the form

$$DF(x) = 0 \quad x \in \mathbb{R}^3, x_3 > 0 \quad (3.24)$$

$$\Re(F(x_1, x_2)) = f(x_1, x_2) \quad x_1, x_2 \in \mathbb{R}^2 \quad (3.25)$$

To solve this problem we follow the same idea as above.

$$F_\Gamma f = \int_{\mathbb{R}^2} \frac{x-y}{|x-y|^2} e_3 f(x_1, x_2) dx_1 dx_2 \quad (3.26)$$

$$\begin{aligned} \text{tr} F_\Gamma f &= \frac{1}{2}(I + S_\Gamma)f = \frac{1}{2}f(\tilde{y}_1, \tilde{y}_2) \\ &\quad + \frac{1}{2} \int_{\mathbb{R}^2} \frac{\mathbf{e}_1(x_1 - \tilde{y}_1) + \mathbf{e}_2(x_2 - \tilde{y}_2)}{|x-y|^2} e_3 f(x_1, x_2) dx_1 dx_2. \end{aligned} \quad (3.27)$$

Because the quaternions \mathbb{H} are isomorphic to the even subalgebra $C\ell_{0,3}^+$, *i.e.* all elements of the form

$$c_0 + c_1 e_1 e_2 + c_2 e_1 e_3 + c_3 e_2 e_3, \quad c_0, c_1, c_2, c_3 \in \mathbb{R} \quad (3.28)$$

we can set $\mathbf{i} = \mathbf{e}_1 \mathbf{e}_2$ and $\mathbf{j} = \mathbf{e}_2 \mathbf{e}_3$ so that

$$\text{tr} F_\Gamma f = \frac{1}{2}(I + S_\Gamma)f \quad (3.29)$$

$$= \frac{1}{2}f(\tilde{y}_1, \tilde{y}_2) + \frac{1}{2} \int_{\mathbb{R}^2} \frac{\mathbf{i}(x_1 - \tilde{y}_1) + \mathbf{j}(x_2 - \tilde{y}_2)}{|x-y|^2} f(x_1, x_2) dx_1 dx_2. \quad (3.30)$$

Up to the factor 1/2 this is the monogenic signal $f_M = f + \mathbf{i}\mathcal{R}_1 f + \mathbf{j}\mathcal{R}_2 f := f + (\mathbf{i}, \mathbf{j})\mathcal{R} f$ of Sommer and Felsberg [9]. Here \mathcal{R}_1 , \mathcal{R}_2 and \mathcal{R} denote respectively the first and second component of the Riesz transform, and the Riesz transform itself [22]. Defined as Fourier multipliers, it holds:

$$\widehat{\mathcal{R}f}(u_1, u_2) = \frac{i(u_1, u_2)}{\|(u_1, u_2)\|_2} \widehat{f}(u_1, u_2) \quad (3.31)$$

$$\widehat{\mathcal{R}_1 f}(u_1, u_2) = \frac{iu_1}{\|(u_1, u_2)\|_2} \widehat{f}(u_1, u_2) \quad (3.32)$$

$$\widehat{\mathcal{R}_2 f}(u_1, u_2) = \frac{iu_2}{\|(u_1, u_2)\|_2} \widehat{f}(u_1, u_2) \quad (3.33)$$

where $\|(u_1, u_2)\|_2 = \sqrt{u_1^2 + u_2^2}$.

or equivalently defined in the spatial domain by convolution with the 2-dimensional Riesz kernel, for $m = 1, 2$

$$\mathcal{R}_i f = c \frac{x_i}{\|x\|_2^3} * f \quad (3.34)$$

with c being a constant.

3.2.2. Image analysis. Following [9] three features can be computed and will be denoted as *energetic, structural and geometrical information* too, as already introduced for the multidimensional analytic signal.

Amplitude. The local amplitude of a monogenic signal is defined in a similar way as for the analytic signal:

$$A_M(x, y) = \sqrt{|f(x, y)|^2 + |\mathcal{R}f(x, y)|^2} = \sqrt{f_M(x, y)\bar{f}_M(x, y)} \quad (3.35)$$

where the $\bar{\cdot}$ denotes the conjugation of a quaternion.

Phase.

$$\phi_M(x, y) = \arctan \frac{|\mathcal{R}f(x, y)|}{|f(x, y)|} \quad (3.36)$$

and we still have that ϕ_M denotes the angle between $A(x, y)$ and f_M (in the plane spanned by the two complex vectors). This yields values $\phi_M \in [-\pi/2; \pi/2]$

An alternative equivalent definition is using \arccos :

$$\phi_M = \arccos \frac{f}{|f_M|} \quad (3.37)$$

In this case, we have $\phi_M \in [0; \pi]$

Orientation. Once again, we can derive an orientation $\theta_M \in [-\pi, \pi]$ based on the monogenic signal which represents the direction of the phase information.

$$\theta_M = \arctan \frac{\mathcal{R}_2 f}{\mathcal{R}_1 f} \quad (3.38)$$

We note that this definition actually only provides an orientation mod. π . To determine the orientation resp. direction mod. 2π it needs a further orientation unwrapping step or sign estimation [17, 4].

3.3. Illustrations

We want here to illustrate the differences between the generalizations proposed. We will visually assess the characteristics of both approaches first facing a Siemens star¹ then facing a checkerboard image. Both examples are interesting for their regularity (point symmetry for the star and many horizontal and vertical line symmetries for the checkerboard).

An example of such star is depicted on Fig. 2(a). The two other images of first row from Fig. 2 illustrate the two components of the Riesz transform. As we can see, and we will come back on that property later, the partial Riesz transforms show in some point a similar behavior as steered derivatives. The first component tends to emphasize horizontal edges while the second one tends to respond more to vertical ones.

The second row shows the results applying the different Hilbert transforms to the Siemens star. The two first images represent the results of the

¹The Siemens star is a known test image to characterize the resolution of different optical/graphical devices such as printers or beamers. It is interesting as it shows lots of regularity, many intrinsic one dimensional and two dimensional parts.

two partial Hilbert transforms and the last one depicts the results after the total Hilbert transform. We can notice the high anisotropy of these transforms at, for instance, the strong vertical resp. horizontal delimitation through the centers of the images. We can also notice the patchy responses of the total Hilbert transform.

As the Riesz kernel in polar coordinate $[r, \alpha]$ of the spatial domain reads

$$R(r, \alpha) \sim \frac{1}{r^2} e^{i\alpha} \quad (3.39)$$

it exhibits an isotropic behavior with respect to its magnitude. In comparison, the partial and the total Hilbert transforms induce a strict relationship to the orthogonal coordinate system and therefore also the two-dimensional analytic signal is coined in such a way.

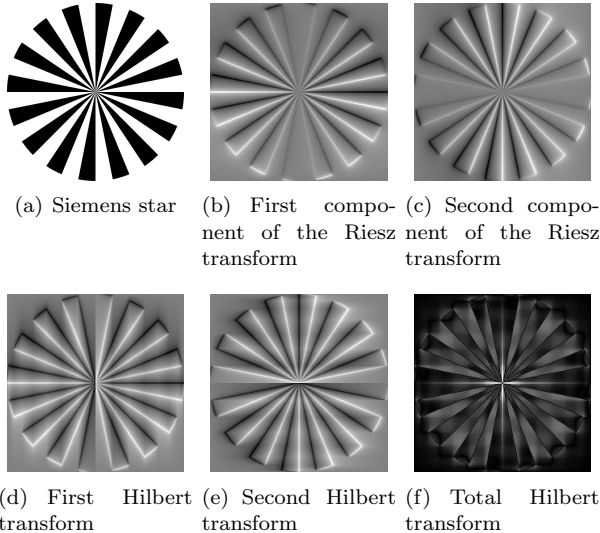


FIGURE 2. The Siemens star together with the different Riesz and Hilbert transforms presented in this section.

Next we consider the local features computed according to the formulas introduced above. The results are depicted in Fig. 3. The first row corresponds to monogenic features, while the second one corresponds to analytic features. The phase is displayed in a jet colormap, the orientation in an hsv colormap. The last column shows the orientations whose intensity is weighted proportionally to the cosine of the phase. It is shown according to Middlebury's representation²: strength (cosine of the phase) is encoded as an intensity value of the color and the color itself corresponds to the orientation.

²Middlebury benchmark for optical flow is a web resource for comparing results on optical flow computations. The color error representation is well suited for encoding our orientation. More info can be found at <http://vision.middlebury.edu/flow/>

The main differences between these two sets of features lie in the shape or boundaries. While monogenic features yield rather smooth boundaries, the analytic representation creates abrupt changes due to its anisotropy. We can remark how the phase gives reasonable insights about the structures in the images.

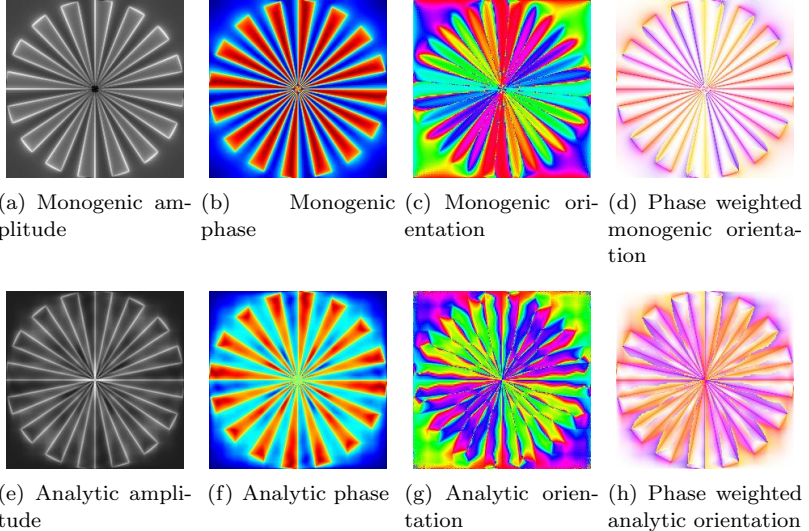


FIGURE 3. Local features computed with the monogenic signal representation (first row) and the multidimensional analytic signal (second row). The images are depicted in pseudo-color representation; amplitude: gray; phase: jet; orientation: hsv-Middlebury.

In comparison to the Siemens star, the checkerboard example (see Fig. 4(a)) shows many orthogonal features. In this case, we see that the partial Hilbert transforms give some good insights of the closeness of an edge and preserves the checkerboard structure (Fig. 4(d) and 4(e)) while the Riesz transform gives more local responses. The total Hilbert transform acts as an accurate corner detection, as it can be seen from its response on Fig. 4(f).

When discussing the analytic and monogenic features (Fig. 5) we remark that this effect is preserved. The Riesz transform being well localized at the edges does not yield many differences inside one of the square and seems to jump from an extreme to another through those edges. See in particular Fig. 5(b) for an illustrative example of the phase. On the other side, the Hilbert transform containing more neighborhood information yields smoother transition in the phase from a square to another. This idea has to be considered carefully based on the applications one wants to solve.

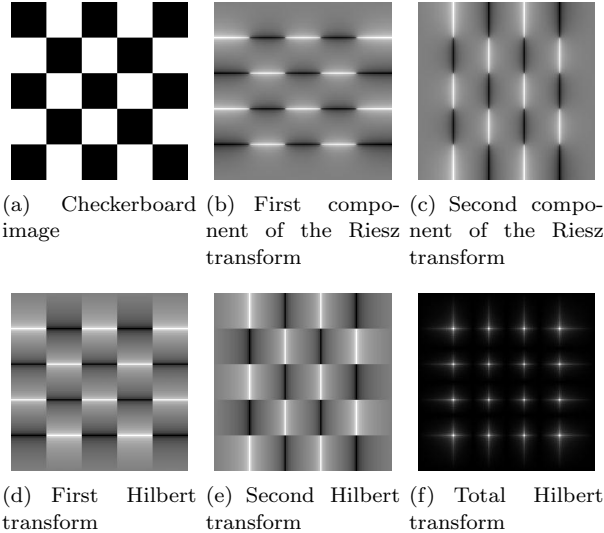


FIGURE 4. The checkerboard together with the different Riesz and Hilbert transforms presented in this section.

4. The geometric approach

For a better understanding of signals a geometric interpretation of a signal can help. The following considerations about complex numbers, quaternions, rotations, the unitary group, the special unitary and special orthogonal group as well as the spin group are well-known and can be found in numerous papers. We would like to suggest the book [18], as a comprehensive insight in the topic. The analytic signal $f_A(t) = A(t)e^{i\phi(t)}$ are boundary values of an analytic function, but the analytic signal can also be seen as a complex number, where $e^{i\phi(t)} = \cos \phi(t) + i \sin \phi(t)$ has modulus 1 and hence can be identified with the unit circle S^1 . But there is even more. The set of unit complex numbers becomes a group with the complex multiplication which is the unitary group $U(1) = \{z \in \mathbb{C} : z\bar{z} = 1\}$. On the other hand a unit complex number can also be seen as a rotation in \mathbb{R}^2 if we identify the unit complex number with the matrix

$$R_\phi = \begin{pmatrix} \cos \phi & -\sin \phi \\ \sin \phi & \cos \phi \end{pmatrix} \in SO(2) \quad (4.1)$$

the group of all counter-clockwise rotations in \mathbb{R}^2 . Now everything can also be described inside Clifford algebras. Let us consider the Clifford algebra $C\ell_{0,2}$ with generators e_1, e_2 . The complex numbers can be identified with all elements $x + ye_{12}$, $x, y \in \mathbb{R}$, i.e. the even subalgebra $C\ell_{0,2}^+$ of the Clifford algebra $C\ell_{0,2}$. The rotation (4.1) can also be described by a Clifford multiplication. To see that we identify $(x, y) \in \mathbb{R}^2$ with $xe_1 + ye_2 \in C\ell_{0,2}$ and

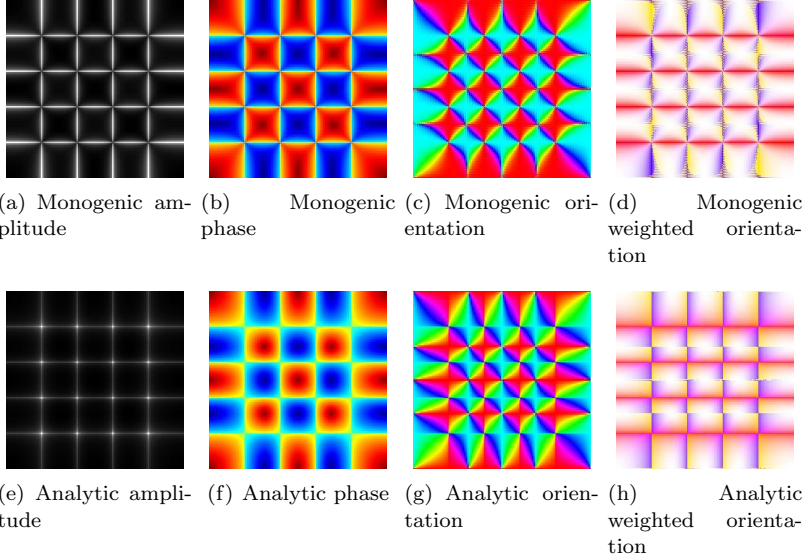


FIGURE 5. Local features computed with the monogenic signal representation (first row) and the multidimensional analytic signal (second row). The images are depicted in pseudo-color representation; amplitude: gray; phase: jet; orientation: hsv-Middlebury.

$$R_\phi(x, y)^T = (\cos \frac{\phi}{2} + e_{12} \sin \frac{\phi}{2})^{-1} (x e_1 + y e_2) (\cos \frac{\phi}{2} + e_{12} \sin \frac{\phi}{2}), \quad (4.2)$$

where $\cos \frac{\phi}{2} + e_{12} \sin \frac{\phi}{2} \in \text{Spin}(2) = \{s \in C\ell_{0,2}^+ : s\bar{s} = 1\}$, the spin group of even products of Clifford vectors. It is easily seen that s and s^{-1} from $\text{Spin}(2)$ represent the same rotation, which means that $\text{Spin}(2)$ is a two-fold cover of $SO(2)$. The basis for all these interpretations is still the description of complex numbers in a trigonometric way, which is possible by using a logarithm function which is well-known for complex numbers. All of that can be generalized into higher dimensions and has been used for monogenic signals. We will start with quaternions because they are the even subalgebra of the Clifford algebra $C\ell_{0,3}$.

4.1. Quaternions and rotations

A quaternion $q \in \mathbb{H}$ can be written as

$$q = q_0 + \underline{q} = S(q) + \mathbf{V}(q) = |q| \frac{\underline{q}}{|q|}, \quad (4.3)$$

where $|q|$ is the absolute value or norm of q in \mathbb{R}^4 and $\frac{\underline{q}}{|q|} \in \mathbb{H}_1$ is a unit quaternion.

Because of

$$\left| \frac{q}{|q|} \right|^2 = \sum_{i=0}^3 \frac{q_i^2}{|q|^2} = 1, \quad (4.4)$$

the set of unit quaternions \mathbb{H}_1 can be identified with S^3 , the three dimensional sphere in \mathbb{R}^4 .

On the other hand the Clifford algebra $\mathcal{C}\ell_{0,3}$ is generated by the elements e_1, e_2 and e_3 with $e_1^2 = e_2^2 = e_3^2 = -1$ and $e_i e_j + e_j e_i = -2\delta_{i,j}$. Its even subalgebra $\mathcal{C}\ell_{0,3}^+$, as defined in 3.28, can be identified with quaternions by $e_1 e_2 \sim \mathbf{i}, e_1 e_3 \sim \mathbf{j}$ and $e_2 e_3 \sim \mathbf{k}$.

Furthermore,

$$\text{Spin}(3) = \{u \in \mathcal{C}\ell_{0,3}^+ : u\bar{u} = 1\} = \mathbb{H}_1. \quad (4.5)$$

That means a unit quaternion can be considered as a spinor. Because $\text{Spin}(3)$ is a double cover of the group $SO(3)$, rotations can be described by unit quaternions. The monogenic signal is interpreted as a spinor in [24] and lately in [1].

4.2. Quaternions in trigonometric form

The analytic signal is a holomorphic/analytic function and therefore connected to complex numbers. Complex numbers can be written in algebraic or trigonometric form:

$$z = x + iy = re^{i\phi}.$$

The analytic signal is given by

$$A(t)e^{i\phi(t)}$$

with amplitude $A(t)$ and (local) phase $\phi(t)$. We want to obtain a similar representation of the monogenic signal by quaternions. A simple computation leads to

$$q = |q| \left(\frac{q_0}{|q|} + \frac{\underline{q}}{|q|} \frac{|q|}{|q|} \right) = |q|(\cos \phi + \underline{u} \sin \phi),$$

where $\phi = \arccos \frac{q_0}{|q|}$ and $\underline{u} = \frac{\underline{q}}{|q|} \in S^2$. (Alternatively, the argument ϕ can be defined by the arctan.)

We can represent the quaternion q by its amplitude $|q|$, the phase ϕ and the orientation \underline{u} . Moreover,

$$q = |q| e^{\underline{u}\phi},$$

where e is the usual exponential function.

By the aid of an appropriate logarithm we can compute $\underline{u}\phi$ from $\frac{q}{|q|} = e^{\underline{u}\phi}$. Next, we want to explain the orientation \underline{u} . We already got that

$$q = |q|(\cos \phi + \underline{u} \sin \phi),$$

where $\underline{u} = \frac{q}{|q|} \in S^2$ and $\underline{u}^2 = -1$, i.e. \underline{u} behaves like a complex unit. But because $\underline{u} \in S^2$ we can express \underline{u} in spherical coordinates. We have

$$\underline{u} = \frac{q_1 \mathbf{i} + q_2 \mathbf{j} + q_3 \mathbf{k}}{|q_1 \mathbf{i} + q_2 \mathbf{j} + q_3 \mathbf{k}|} = \mathbf{i} \left(\frac{q_1}{|q|} + \frac{(q_2(-\mathbf{i}\mathbf{j}) + q_3\mathbf{j})}{|q|} \right) \quad (4.6)$$

and if we set $\cos \theta = \frac{q_1}{|q|}$ we get

$$\underline{u} = \mathbf{i}(\cos \theta + \underline{u} \sin \theta), \quad \underline{u} = \frac{\underline{q}}{|q|} \text{ and } \underline{q} = \mathbf{j}q_3 - \mathbf{i}jq_2. \quad (4.7)$$

Because of

$$\underline{q} = \mathbf{j}q_3 - \mathbf{i}jq_2 = \mathbf{j}(q_3 + iq_2) \quad (4.8)$$

and with $\cos \tau = \frac{q_3}{|q|}$ we get that

$$\underline{u} = \mathbf{j}(\cos \tau + \mathbf{i} \sin \tau). \quad (4.9)$$

Finally, we put everything together and obtain

$$q = q_0 + q_1\mathbf{i} + q_2\mathbf{j} + q_3\mathbf{k} \quad (4.10)$$

$$= |q|(\cos \phi + \underline{u} \sin \phi) = |q|(\cos \phi + \mathbf{i}(\cos \theta + \underline{u} \sin \theta) \sin \phi) \quad (4.11)$$

$$= |q|(\cos \phi + \mathbf{i}(\cos \theta + \mathbf{j}(\cos \tau + \mathbf{i} \sin \tau) \sin \theta) \sin \phi) \quad (4.12)$$

$$= |q|(\cos \phi + \mathbf{i} \sin \phi \cos \theta + \mathbf{j} \sin \phi \sin \theta \sin \tau + \mathbf{k} \sin \phi \sin \theta \cos \tau), \quad (4.13)$$

where $\phi, \theta \in [0, \pi]$ and $\tau \in [0, 2\pi]$. In case of a reduced quaternion, i.e. $q_3 = 0$, a similar computation leads to

$$q = q_0 + q_1\mathbf{i} + q_2\mathbf{j} \quad (4.14)$$

$$= |q|(\cos \phi + \underline{u} \sin \phi) = |q|(\cos \phi + \mathbf{i}(\cos \theta - \mathbf{k} \sin \theta) \sin \phi) \quad (4.15)$$

$$= |q|(\cos \phi + \mathbf{i} \sin \phi \cos \theta + \mathbf{j} \sin \phi \sin \theta), \quad (4.16)$$

where $\phi \in [0, \pi]$ and $\theta \in [0, 2\pi]$.

It is easily seen that θ can be computed by

$$\tan \theta = \frac{q_2}{q_1} \iff \theta = \arctan \frac{q_2}{q_1}.$$

If we compare that with the monogenic signal

$$f_M(x, y) = f(x, y) + \mathbf{i}(\mathcal{R}_1 f)(x, y) + \mathbf{j}(\mathcal{R}_2 f)(x, y)$$

we see that (compare with 3.38)

$$\theta = \arctan \frac{(\mathcal{R}_2 f)(x, y)}{(\mathcal{R}_1 f)(x, y)} = \theta_M(x, y). \quad (4.17)$$

Therefore the vector $\underline{u} = \mathbf{i} \cos \theta + \mathbf{j} \sin \theta$ can also be considered as the orientation.

4.3. Exponential function and logarithm for quaternionic arguments

The exponential function for quaternions and para-vectors in a Clifford algebra are defined in [11] and many other papers.

Definition 4.1. For $q \in \mathbb{H}$ is the exponential function defined as

$$e^q := \sum_{k=0}^{\infty} \frac{q^k}{k!}. \quad (4.18)$$

Lemma 4.2. With $\underline{u} = \frac{q}{|q|}$ the exponential function can be written as

$$e^q = e^{q_0} (\cos |q| + \underline{u} \sin |q|) = e^{q_0} e^{\underline{u}|q|}. \quad (4.19)$$

Remark 4.3. The formula

$$e^{\underline{u}|q|} = \cos |q| + \underline{u} \sin |q| \quad (4.20)$$

can be considered as a generalized Euler formula.

It is always a challenge to define a logarithm. We will use the following definition.

Definition 4.4. Let $\underline{u} = \frac{q}{|q|}$, then the logarithm is defined as

$$\ln q := \begin{cases} \ln |q| + \underline{u} \left(\arccos \frac{q_0}{|q|} \right), & |\underline{q}| \neq 0 \text{ or } |q| = 0 \text{ and } q_0 > 0, \\ \text{not defined for } |\underline{q}| = 0 \text{ and } q_0 \leq 0. \end{cases} \quad (4.21)$$

Remark 4.5. A logarithm cannot be uniquely defined for -1 because

$$e^{\underline{u}\pi} = \cos \pi + \underline{u} \sin \pi = -1, \quad (4.22)$$

for all $\underline{u} \in S^2$.

Remark 4.6. More precise, we can define the k -th branch, $k \in \mathbb{Z}$, of the logarithm because $\cos t$ is a 2π periodic function.

Theorem 4.7. 1. For $|\underline{q}| \neq 0$ or $|\underline{q}| = 0$ and $q_0 > 0$,

$$e^{\ln q} = q. \quad (4.23)$$

2. For $|\underline{q}| \neq k\pi$, $k \in \mathbb{Z} \setminus \{0\}$ it holds true

$$\ln e^q = q. \quad (4.24)$$

Lemma 4.8. For $q \in \mathbb{H}_1$ and $q \neq -1$ both relations are true:

$$e^{\ln q} = \ln e^q = q. \quad (4.25)$$

5. Applications to image analysis

5.1. Motivations

In several imaging applications only intensity-based images (encoded mostly in gray-scale representation) are provided. Apart from monochromatic camera images, we can cite *e.g.* computerized tomography images which encodes local absorption inside a body, or optical coherence tomography images which represents the back-scattering at an interface. These kind of images describe natural scenes or physical quantities directly. In other types of images information is encoded indirectly, *e.g.* in varying amplitude or frequency of fringe patterns. They are called amplitude modulated (AM) or frequency modulated (FM) signals. Textures can be interpreted as a trade-off between both ideas: they depict natural scenes and can be described as generalized AM-FM signals.

To enrich the information content of pure intensity image (*i.e.* images encoded with a single value at each pixel), we test the concept of analytic signals in image processing.

5.2. Application to AM-FM images demodulation

Here we study the applicability of the monogenic signal representation to AM-FM signal demodulation, as needed for instance in interferometric imaging [17]. A certain given two dimensional signal (= an image, Fig. 6(a)) exhibits both amplitude modulations (Fig. 6(b)) and frequency modulations (Fig. 6(c)). The aim is to separate each components of the signal by means of monogenic signal analysis.

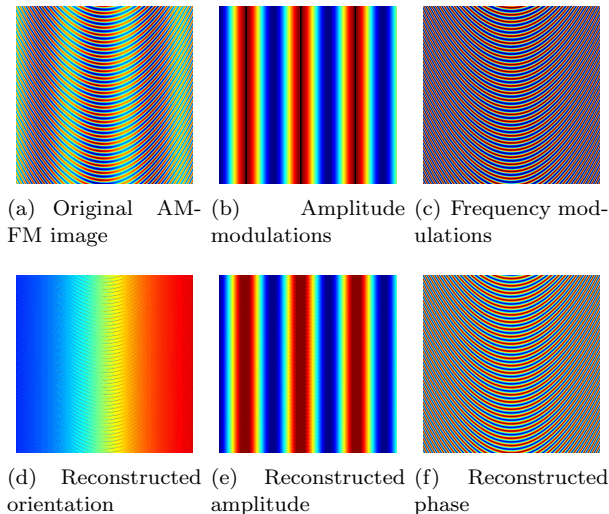


FIGURE 6. Example of a two dimensional AM-FM signal. The first row shows the input ground truth image together with its amplitude and frequency modulations. The second row depicts the recovered orientation, amplitude and phases. Images are displayed using conventional jet colormap.

The three features described in the previous section are computed and their results are depicted on Fig. 6(d) (local orientation), Fig. 6(e) (local amplitude) and Fig. 6(f) (local phase).

It appears that on such AM-FM signals, the orientation is able to describe the direction of the phase modulation, while the local amplitude gives a good approximation of the amplitude modulation (corresponding to the energy of the two dimensional signal) and the phase encodes information about the frequency modulation (understood as the structural information).

The next example shows a fringe pattern as an example of real-world interferometric AM-FM image, Fig. 7(a).

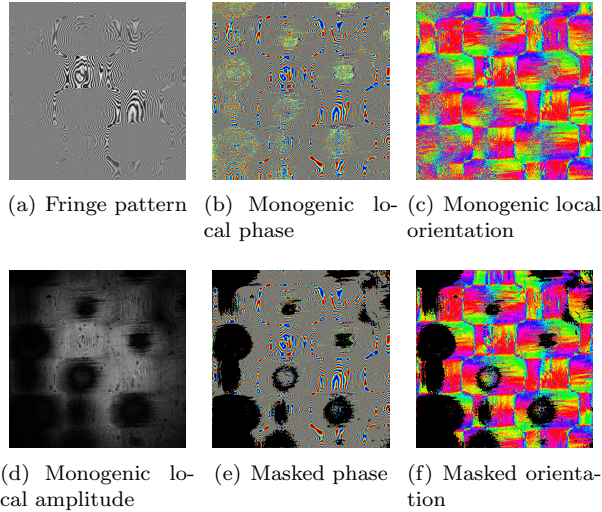


FIGURE 7. Example of a fringe pattern and its monogenic decomposition. Phase (second column) is encoded as a jet colormap and orientation as hsv. The two last images show phase and orientation masked with a binary filter set to one when the local amplitude gets over a certain threshold.

The following images show the monogenic analysis of this image. Beneath the fringe pattern (Fig. 7(d)) the local amplitude is depicted. This image gives us a coarse idea of how much structure is to be found on a given neighborhood. The second column illustrates the phase calculation either on the whole image (Fig. 7(b)) or only where the local amplitude is above a given threshold (Fig. 7(e)). The two last images represent the monogenic orientation encoded in hsv with or without the previous mask. As we would expect, illumination changes are appearing in the amplitude while local structures are contained in both phase and orientation features.

5.3. Application to texture analysis

A task of particular interest in artificial vision, is the characterization or description of textures. The problem here is to find interesting features to describe a given texture the best we can in order to classify it for instance [13]. The use of steerable filters could optimize the feature computations and affect the classification. In other words, if we can compute well describing features, we can better characterize a texture.

Considering textures from a more general viewpoint as almost AM-FM signals, we examine here the use of monogenic representation for local characterization of a textured object depicted in Fig. 8(a).

When looking at the monogenic signal's local description (amplitude on Fig. 8(b), phase on Fig. 8(c) and orientation on Fig. 8(d)) we indeed see

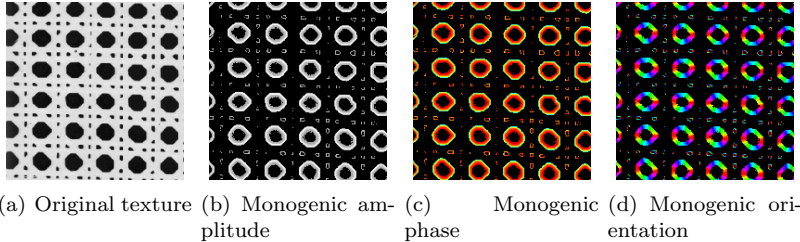


FIGURE 8. Example of a textured image superposed by a reliability mask together with its monogenic analysis; regions with too little amplitude are masked out to be unreliable.

these repetitive features along the textured object. Moreover, these estimated values seem to be robust against small imperfection in the periodicity.

5.4. Applications to natural image scenes

In this part of work, we want to give some ideas of the interest of the monogenic signal for natural images. Such images have completely different characteristics as the ones introduced above. For instance, images are often embedded in full cluttered background, encoded on more color channels, have information at many different scales... In practical applications one needs to apply band-pass filters before analyzing such images [9]. Note that this work considers only gray-scaled images, but literature can be found in order to deal with multichannel images [2].

We will in the followings describe two tasks useful for image processing. The first part deals with edge detection. We see how the Riesz transform can be used as an edge detector in images. Then we see how the orientation estimation is useful for instance in computer vision tasks and how the monogenic signal analysis can help for this, as it has already been done for structure interpretation [21, 14].

5.4.1. Edge detection. The Riesz transform can be seen as an edge detectors for several reasons. It appears clearly when one has a closer look at its definition as a Fourier multiplier. Indeed, let us recall the j^{th} Riesz multiplier (see Eq. 3.31):

$$\widehat{\mathcal{R}_j f} = i \frac{u_j}{|u|} \widehat{f} \quad (5.1)$$

and we have

$$\widehat{\mathcal{R}_j f} = i \frac{1}{|u|} \widehat{\partial_j f} \quad (5.2)$$

so that the Riesz transform acts as a normalized derivative operator.

Another (eventually better) way to see this derivative effect is to consider the Fourier multipliers in polar coordinates [16], which is given by Eq. 3.39.

Fig. 9 illustrates this behavior.

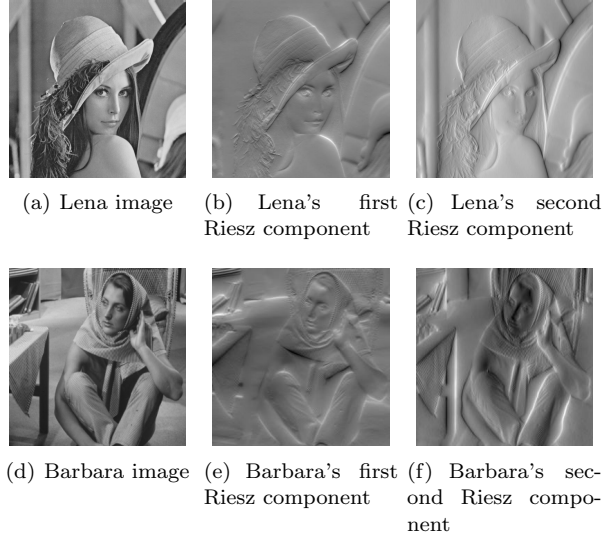


FIGURE 9. First and second components of the Riesz transform on some natural images. Notice for instance the table leg appearing in Fig. 9(f) and not in Fig. 9(e), showing the directions of the components.

The first column shows examples of gray level natural images. The second and third columns show respectively the first and second Riesz component. It appears that they act as edge detection steered in the x and y directions. If we compare the two Riesz components, we can see different kind of edges responding.

5.4.2. Orientation estimation of edges. An important task in image processing and higher level computer vision is to estimate the orientation of edges. As this is often the first step towards features description and image interpretation (we refer the reader to [6, 19] for some non-exhaustive surveys), one wants to have an orientation estimator as reliable as possible.

As stated in earlier sections, an orientation can be computed from an analytic or monogenic signal analysis. For simplicity reasons, let us consider the case of images, where the input function is defined on $D \subset \mathbb{R}^2$. Using the polar coordinate in Fourier domain (ρ, β) , it holds

$$\widehat{\mathcal{R}f} = i(\cos \beta, \sin \beta)^T \widehat{f} \quad (5.3)$$

on the other side, we also have

$$\widehat{\nabla f} = i\rho(\cos \beta, \sin \beta)^T \widehat{f} \quad (5.4)$$

so that both gradient and Riesz operators have a similar effect on the angles in the Fourier domain.

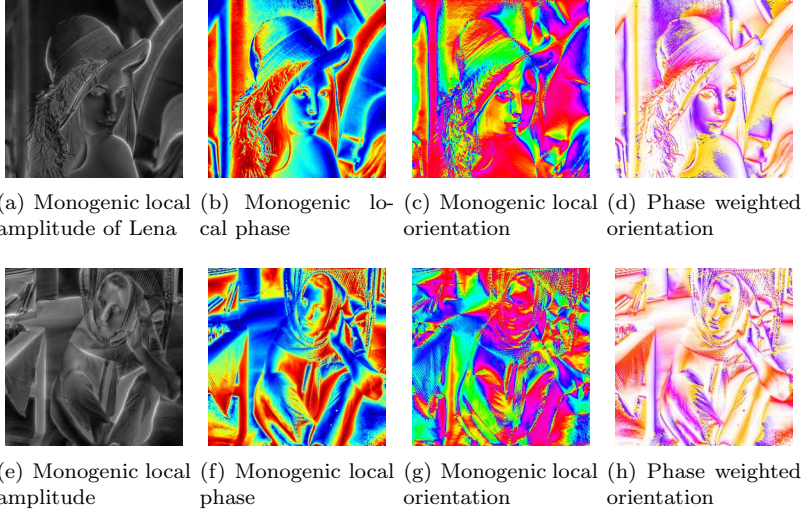


FIGURE 10. Local features computed by means of monogenic signal analysis.

It has been shown [8] that using monogenic orientation estimation increases the robustness compared to the traditional Sobel operator. Moreover in their work Felsberg and Sommer introduced an improved version based on local neighborhood considerations and using the phase as a confidence value.

Fig. 10 illustrates the monogenic analysis of our two test images. The first column represents the local amplitude of the image; the second one shows the local phases according to the monogenic definition. The two last columns illustrate the computation of the monogenic orientation. The colors are encoded on a linear periodic basis according to the Middlebury color coding. The last column shows the exact same orientation but with the importance of the phase as intensity information. The basic idea is to keep relevant orientation only where the structural information (*i.e.* the phase) is high.

Note that we are here not to discuss here the local-zero mean property in natural image scenes. So e.g. background and illumination effects may influence the procedure and will be discussed somewhere else.

6. Conclusion

In this article the specificity and analysis of both generalizations of the analytic signal have been detailed mathematically based respectively on multiple complex analysis and Clifford analysis. It is shown that they are both valid extensions of the one dimensional concept of analytic signal. A main difference between the two approaches is regarding rotation invariance due to the

point symmetric definition of the *sign* function in the case of monogenic approach against the single orthant definition of the multidimensional analytic signal.

In a second part we have illustrated such analytic or monogenic analysis of images on some artificial samples and real-world examples of fringe analysis or texture analysis. In the context of AM-FM signal demodulation the monogenic signal analysis yields a robust decomposition into energetic, structural and geometric information. Finally some ideas for the use of generalized analytic signals in higher-level image processing and computer vision tasks are given showing high potential for further research.

Acknowledgment

We thank the ERASMUS program and the financial support by the Federal Ministry of Economy, Family and Youth and the National Foundation for Research, Technology and Development are gratefully acknowledged. This work was further supported by part by the Austrian Science Fund under grant no. P21496 N23.

References

1. T. Batard and M. Berthier, *The spinor representation of images*, 2011, Preprint.
2. T. Batard, M. Berthier, and C. Saint-Jean, *Clifford fourier transform for color image processing*, Geometric Algebra Computing in Engineering and Computer Science (2008), 135–161.
3. F. Brackx, R. Delanghe, and F. Sommen, *Clifford analysis*, Research notes in mathematics **76** (1982).
4. T. Bülow, D. Pallek, and G. Sommer, *Riesz transform for the isotropic estimation of the local phase of moiré interferograms*, DAGM-Symposium, 2000, pp. 333–340.
5. T. Bülow and G. Sommer, *Hypercomplex signals-a novel extension of the analytic signal to the multidimensional case*, Signal Processing, IEEE Transactions on **49** (2001), no. 11, 2844–2852.
6. V. Chandrasekhar, D.M. Chen, A. Lin, G. Takacs, S.S. Tsai, N.M. Cheung, Y. Reznik, R. Grzeszczuk, and B. Girod, *Comparison of local feature descriptors for mobile visual search*, Image Processing (ICIP), 2010 17th IEEE International Conference on, IEEE, 2010, pp. 3885–3888.
7. A. Dzhuraev, *On riemann–hilbert boundary problem in several complex variables*, Complex Variables and Elliptic Equations **29** (1996), no. 4, 287–303.
8. M. Felsberg and G. Sommer, *A new extension of linear signal processing for estimating local properties and detecting features*, Proceedings of the DAGM 2000 (2000), 195–202.
9. ———, *The monogenic signal*, Signal Processing, IEEE Transactions on **49** (2001), no. 12, 3136–3144.
10. D. Gabor, *Theory of communication*, Electrical Engineers-Part III: Radio and Communication Engineering, Journal of the Institution of **93** (1946), no. 26, 429–441.
11. K. Gürlebeck, K. Habetha, and W. Sprössig, *Holomorphic functions in the plane and n-dimensional space*, Birkhäuser, 2008.
12. S.L. Hahn, *Multidimensional complex signals with single-orthant spectra*, Proceedings of the IEEE **80** (1992), no. 8, 1287–1300.
13. R.M. Haralick, K. Shanmugam, and I.H. Dinstein, *Textural features for image classification*, Systems, Man and Cybernetics, IEEE Transactions on **3** (1973), no. 6, 610–621.
14. B. Heise, S.E. Schausberger, C. Maurer, M. Ritsch-Marte, S. Bernet, and D. Stifter, *Enhancing of structures in coherence probe microscopy imaging*, Proceedings of SPIE, vol. 8335, 2012, p. 83350G.

15. E.M.S. Hitzer, *Quaternion fourier transform on quaternion fields and generalizations*, Advances in Applied Clifford Algebras **17** (2007), no. 3, 497–517.
16. U. Köthe and M. Felsberg, *Riesz-transforms versus derivatives: On the relationship between the boundary tensor and the energy tensor*, Scale Space and PDE Methods in Computer Vision (2005), 179–191.
17. K.G. Larkin, D.J. Bone, and M.A. Oldfield, *Natural demodulation of two-dimensional fringe patterns. i. general background of the spiral phase quadrature transform*, JOSA A **18** (2001), no. 8, 1862–1870.
18. P. Lounesto, *Clifford algebras and spinors*, vol. 286, Cambridge Univ Pr, 2001.
19. K. Mikolajczyk and C. Schmid, *A performance evaluation of local descriptors*, Pattern Analysis and Machine Intelligence, IEEE Transactions on **27** (2005), no. 10, 1615–1630.
20. W. Rudin, *Function theory in the unit ball of \mathbb{C}^n* , Springer, 1980.
21. V. Schlager, S. Schausberger, D. Stifter, and B. Heise, *Coherence probe microscopy imaging and analysis for fiber-reinforced polymers*, Image Analysis (2011), 424–434.
22. E.M. Stein, *Singular integrals and differentiability properties of functions*, vol. 30, Princeton Univ Pr, 1970.
23. J. Ville, *Theorie et applications de la notion de signal analytique (theory and applications of the notion of analytic signal)*, Cables et transmission **2** (1948), no. 1, 61–74.
24. D. Zang and G. Sommer, *Signal modeling for two-dimensional image structures*, Journal of Visual Communication and Image Representation **18** (2007), no. 1, 81–99.

Index

- Analytic signal, 2, 3
 - Local amplitude, 3
 - Local phase, 3
- Two dimensional, 6
 - Local amplitude, 7
 - Local orientation, 7
 - Local phase, 7
- Checkerboard, 12
- Demodulation, 17
- Dirac operator, 7
- Euler formula
 - for quaternions, 16
- Fourier transform, 2
 - quaternionic, 6
- Hilbert transform, 2
 - partial, 6
 - total, 6
- Interferometry, 17
- Monogenic signal, 8
 - Local amplitude, 9
 - Local orientation, 9
 - Local phase, 9
- Plemelj-Sokhotzki formula, 5
- Quaternion
 - Exponential, 15
 - Logarithm, 16
 - Orientation, 14
- Riemann-Hilbert problem, 4
- Riesz transform, 8
- Siemens star, 10
- Sobel operator, 21
- Spin group, 13
- Spinor, 14
- Split of identity, 2, 3
- Texture, 16

Swanhild Bernstein
Technische Universität Bergakademie Freiberg
Fakultät für Mathematik und Informatik
Institut für Angewandte Analysis
D-09596 Freiberg
Germany
e-mail: swanhild.bernstein@math.tu-freiberg.de

Jean-Luc Bouchot
Johannes Kepler University
Department of Knowledge-Based Mathematical Systems, FLLL
Altenbergerstr., 69
A-4040 Linz
Austria
e-mail: jean-luc.bouchot@jku.at

Martin Reinhardt
Technische Universität Bergakademie Freiberg
Fakultät für Mathematik und Informatik
Institut für Angewandte Analysis
D-09596 Freiberg
Germany
e-mail: martin.reinhardt.87@googlemail.com

Bettina Heise
Johannes Kepler University
Department of Knowledge-Based Mathematical Systems, FLLL and
Christian Doppler Laboratory MS-MACH
Center for Surface- and Nanoanalytics, ZONA
Altenbergerstr., 69
A-4040 Linz
Austria
e-mail: bettina.heise@jku.at